Oil & Gas Science and Technology – Rev. IFP, Vol. 62 (2007), No. 6, pp. 799-817

DOI: 10.2516/ogst:2007062

Dossier
Special Issue in Honour of Yves Chauvin
Numéro spécial en l'honneur de Yves Chauvin

Organometallic Nanoparticles of Metals or Metal Oxides*

B. Chaudret and K. Philippot

Laboratoire de Chimie de Coordination, CNRS-UPR 8241, 205 Route de Narbonne, 31077 Toulouse Cedex 04 - France
e-mail: chaudret@lcc-toulouse.fr - karine.philippot@lcc-toulouse.fr

*Dedicated to Yves Chauvin for his exceptional and exemplary contribution to organometallic chemistry and catalysis
Ce manuscrit est dédié à Yves Chauvin pour sa contribution exceptionnelle et exemplaire à la chimie organométallique et à la catalyse

Résumé — Revue sur la synthèse de nanoparticules de métaux et d'oxydes métalliques — Nous présentons dans cet article une revue sur la synthèse de nanoparticules de métaux et d'oxydes métalliques utilisant une approche organométallique et plus précisément des complexes de ligands hydrocarbures comme précurseurs. L'avantage principal de cette approche réside dans la décomposition facile de ces précurseurs qui peut être effectuée dans des conditions douces et qui ne génère aucun polluant potentiel des nanoparticules. Ceci permet le contrôle de la taille, de la forme et de l'état de surface des nanoparticules formées. Les résultats sont présentés par métaux et par mode de stabilisation (polymères, ligands, liquides ioniques). Nous présentons également quelques résultats concernant l'utilisation de cette approche pour la préparation de matériaux hybrides contenant des nanoparticules incluses dans des matrices minérales (membranes d'alumine, silice mésoporeuse). Enfin nous décrivons également une extension de cette approche pour la synthèse directe de nanoparticules en lit fluidisé.

Abstract — Organometallic Nanoparticles of Metals or Metal Oxides *— This paper presents an overview of the results obtained in the synthesis of metal or metal oxide nanoparticles using hydrocarbyl complexes as metal source. The main advantage of using such metal precursors is their easy decomposition that can be achieved in solution and mild conditions. This allows the control of the particles size, shape and surface state in order to reach a monodisperse assembly of particles having the desired property. The results are reported taking into account the nature of the metal as well as in some cases the stabilizing mode (polymers, ligands, ionic liquids). Some results obtained in the deposition of metal nanoparticles within the channels of templates such as alumina membranes and mesoporous silica through a classsical impregnation method are also reported. The last part concerns the preparation of metal nanoparticles supported on a porous support using a fluidized bed.*

LIST OF ACRONYMS

BMI	1-*n*-butyl-3-methylimidazolium
cod	1,5-cyclooctadiene
cot	1,3,5-cyclooctatriene
CVD	chemical vapor deposition
dba	dibenzylideneacetone
EDX	electron X-ray diffraction
HDA	hexadecylamine
HREM	high resolution electron microscopy
PPO	polyphenyleneoxide
PVP	polyvinypyrrolidone
SAED	selected area electron diffraction
TEM	transmission electron microscopy
THT	tetrahydrothiophene
TOPO	triphenylphosphineoxide
WAXS	wide-angle X-ray scattering

INTRODUCTION

An ever-increasing interest is devoted to chemical species of nanometric size [1-9]. This size corresponds to proteins, to organic macromolecules like polymers or dendrimers or to small molecules which self-organize into micelles or vesicles. Inorganic molecular clusters [10] may also reach this size and display interesting physical properties [11]. Inorganic nanoparticles are in this respect of special interest, due to their many properties which may be exploited, up to practical applications. Thus, metal, metal oxide or various metal based compounds display optical, magnetic, electronic and catalytic properties which find applications in topics as diverse as catalysis and other chemical processes, biology, microelectronics or nanoelectronics.

Many methods have been reported in the literature, especially during the past few years [1], which describe the preparation in solution of particles of metal, metal oxides, or metal chalcogenides. However, since the properties of these nano-objects are in general size dependant, it is essential to have a mean to control the particles size and shape in order to reach a monodisperse assembly of particles having the desired property. In addition, depending of the use of the particles, it is important to control their organization in order to be able to address the particles in selected devices. Finally, a large proportion of the atoms present in a nanoparticle are surface atoms, therefore the chemical and physical properties of the nanoparticles will be strongly influenced by the nature of the surface species. It is then essential to control these surface species. In this respect, the well-known reduction methods [12-15] display limitations due to their lack of variability. The use of reverse micelles as "nanoreactors" inside which salt reduction and particle growth occurs has allowed to obtain monodisperse nano-objects which may display a define shape (spheres, rods, wires) and which may self-assemble on various substrates [16, 17]. In these processes, salt and water are always in contact with the surface of the particles thus passivating them, modifying their reactivity and, in some cases, leading to the production of oxides or hydroxides.

The use of an organometallic precursor, able to decompose either spontaneously or in the presence of a reducing gas, has appeared as a valuable alternative for the synthesis of nano-sized objects [18-20]. Two main advantages can be foreseen when using organometallic precursors:

– the metal is pre-reduced, either in a low oxidation state (preferably zerovalent) or in a formal oxidation state which nevertheless corresponds to a net reduction of the metal (e.g. linked to hydride or alkyl ligands);
– the displacement of suitable organic ligands in mild conditions should afford a surface not containing contaminants detrimental for the chemical or physical properties of the resulting nano-objects.

The first point has led to consider carbonyl complexes as precursors for metal nanoparticles. They may be decomposed thermally in solution to produce fine powders or metal nanoparticles but generally at high temperature. The thermolysis of carbonyl precursors has been largely employed for the preparation of nanoparticles of interest in physics and material science whereas the use of somewhat more sophisticated precursors has interested mainly the field of catalysis [21]. They may also be decomposed by other techniques, namely UV irradiation or sonolysis.

In order to be able to obtain a better control of the size and size distribution of the particles as well as to obtain clean surfaces for undertaking a reproducible chemistry, an alternative approach may be developed, based on the use of organometallic precursors able to decompose in mild conditions, generally using a reducing gas.

We will hereafter present our approach concerning the use of hydrocarbyl precursors for the synthesis of "organometallic nanoparticles" of metal, mainly noble metals, and oxides as well as some relevant results from the literature.

1 SYNTHESIS OF METAL NANOPARTICLES FROM HYDROCARBYL COMPLEXES

An organometallic approach has been developed for the past 15 years taking profit of the intrinsic reactivity of metal complexes towards ligand displacement or ligand reduction [18, 19]. In this case, the reactions may take place in very mild conditions (room temperature or below) and a rigorous control of the surface species may be achieved. The ideal precursor is an organometallic complex containing an olefinic or polyolefinic ligand able either to be hydrogenated to give a bare metal atom that would condense in the reaction medium or to be substituted by CO to give an unstable intermediate. Prototypes of such complexes are $Ru(C_8H_{10})(C_8H_{12})$ and

$Ni(C_8H_{12})_2$ which decompose satisfactorily under dihydrogen in mild conditions *(Scheme 1)*. Complexes accommodating alkyl, allylic or cyclopentadienyl groups may also decompose easily, for example $PtMe_2(C_8H_{12})$, $Co(C_8H_{13})(C_8H_{12})$, $Rh(C_3H_5)_3$ $CpCu^tBuNC$ or $CpIr(C_8H_{12})$. More complex structures may however be used when such olefinic precursors are not available or difficult to obtain. For example, $M(dba)_2$ (dba = dibenzylidene acetone; M = Pd; Pt) is a good precursor for the preparation of nanoparticles of Pd or Pt after treatment with dihydrogen or carbon monoxide. Mixed complexes such as $Rh(acac)(C_8H_{12})$ (acac = $(CH_3CO)_2CH$) also decompose in mild conditions but release potential ligands of the particles namely acacH or the corresponding diol after hydrogenation which may or may not perturb the surface.

For clarity, the results obtained on noble metals, magnetic metals and other metals and main group elements will be reported separately. The chosen examples will allow the presentation of the different stabilization modes that can be used with this method to get well-defined nanoparticles.

1.1 Organometallic Synthesis of Noble Metal Nanoparticles

1.1.1 Stabilization by Polymers

$Ru(C_8H_{10})(C_8H_{12})$ (2) reacts rapidly with dihydrogen (1-3 atm) at room temperature in an hydrocarbon solvent to give ruthenium particles and cyclooctane [22]. In the presence of a polymer (polyvinylpyrrolidone, PVP; nitrocellulose, NC; cellulose acetate, CA), the reaction produces particles, the size of which depends upon the nature of the polymer and upon the relative concentration of the precursor in the polymer. In this way, monodisperse particles of 1 to 1.5 nm mean size have been prepared in PVP or NC. In both cases, the particles display very low size dispersity. In contrast, the reaction in CA produces larger particles displaying a broader size dispersity, which evidences the influence of the nature of the polymer and of its coordination ability on the stabilization of the particles. The particles in PVP were analysed by TEM and HREM *(Fig. 1a, b)* and WAXS [23]. The particles adopt the hcp structure of bulk ruthenium. An interesting effect of the size reduction on the crystal lattice has been evidenced. A contraction of 1.1% in the metal-metal distance (0.266 nm, 0.27058 in the bulk) is observed together with a relaxation of the *c* parameter (0.436 nm, 0.42811 in the bulk) which leads to a *c*/*a* ratio of 1.633 close to the ideal one instead of 1.582 in bulk ruthenium.

Palladium nanoparticles can easily be prepared by displacement of the olefinic ligands by dibenzylidene acetone from $Pd(dba)_2$. An intermediate unstable carbonyl complex forms which collapses into clusters. By this method, palladium nanoparticles of sizes in the range 2-5 nm could be obtained using polyvinylpyrrolidone (PVP) [24] or cellulose derivatives [25] as stabilizers. Such particles were recently used to probe the mechanism of the Heck reaction. A correlation between the initial reaction rate and the particle sizes was established. The small particles proved more active in agreement with the presence of more surface palladium atoms with low metal-metal coordination number [26].

In a very similar way, platinum particles were prepared by displacement of dba by CO from $Pt(dba)_2$. In this case, if the reaction is carried out in THF, no stabilizer is necessary and stable particles of ca 1.5 nm form in solution [27].

The particles adopt the fcc structure of platinum with, in the case of particles prepared in the presence of PVP, a contraction of the Pt-Pt distance of 1.2% (0.274 nm) compared to the bulk. These lattice effects are similar to what may be observed in high vacuum and evidence the lack of stress experienced by the particles in these media [28]. The

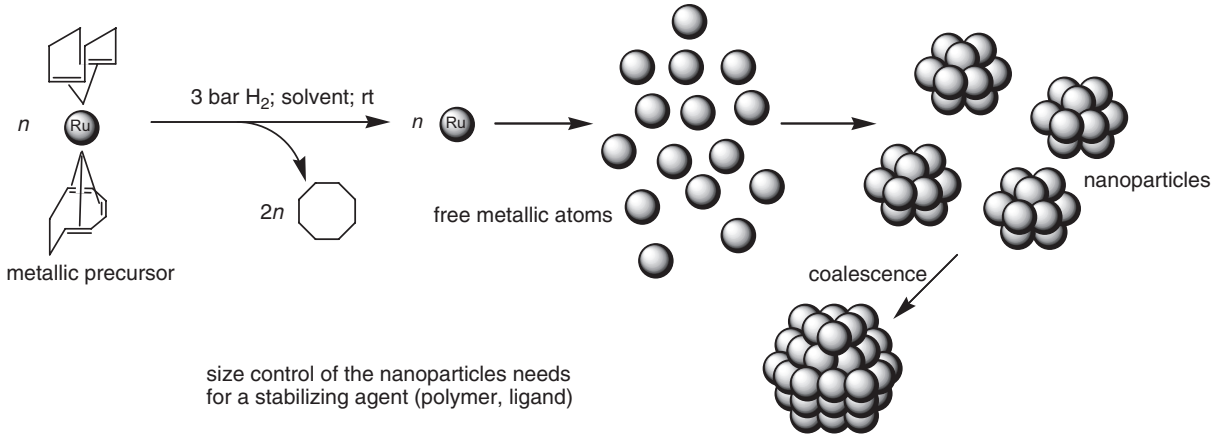

Scheme 1

Schematic representation of the organometallic approach for the synthesis of metal nanoparticles from $Ru(C_8H_{10})(C_8H_{12})$.

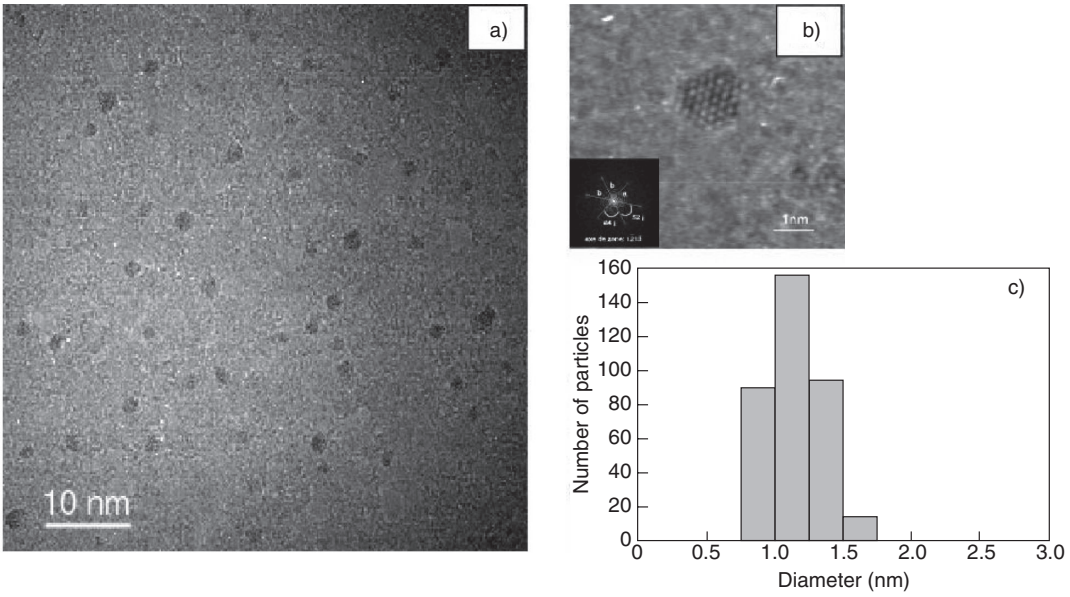

Figure 1

a) TEM micrograph; b) HREM micrograph showing a well-crystallized particle and c) size histogram (mean size ca. 1.1 nm) of Ru nanoparticles embedded in PVP (Adapted from Reference 28).

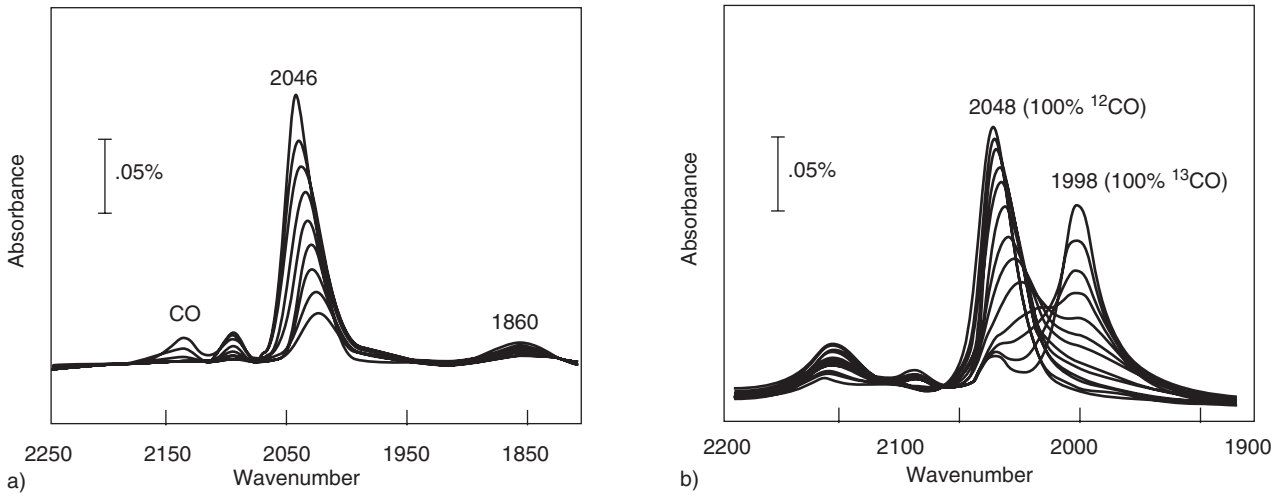

Figure 2

Infrared spectra of CO a) and of $^{13}CO/^{12}CO$ b) adsorbed on 1.5 nm Pt/PVP in dichloromethane (Adapted from Reference 29).

structure of the surface of such Pt particles was investigated by infrared spectroscopy of adsorbed CO *(Fig. 2)* [29]. The presence of vibrational couplings between CO groups attached to a face of the particles was evidenced. This experiment shows the similarity between the particles prepared in organic solutions and the clean metal surfaces in ultra high vacuum (UHV) [30]. PVP coated particles of this type were embedded into an amorphous microporous titania-silica mixed oxide by means of a modified sol-gel procedure. The resulting material was found more selective than both the PVP coated nanoparticles in solution and platinum particles on the mixed oxide without polymer for the hydrogenation of 2-hexyne into cis-2-hexene [31].

Co-decomposition of $Ru(C_8H_{10})(C_8H_{12})$ and $Pt(dba)_2$ leads to the formation of bimetallic Ru_x-Pt_{1-x} particles [32]. Platinum rich particles are fcc whereas ruthenium rich ones are hcp. There is a critical composition Ru_3-Pt for which most of the particles are twinned. In this case, the particles are monodisperse and very small (1.1 nm). This composition corresponds roughly to the limit of solubility of ruthenium in

the platinum lattice for bulk alloys. The particles adopt a twinned fcc structure with the twinning wall lying in a (111) plane located in the middle of the particle. The homogeneity in the size and shape of the twinned particles suggests a well-defined atomic organization: namely a twinned truncated octahedron for the particles which can also be described as well-defined clusters.

Palladium and platinum nanoparticles may be prepared in a block copolymer. The complexes: Pd[endo-2-(cyclopentadienylmethyl)norborn-5-ene](1-phenylallyl) and $PtMe_3$ [endo-2-(cyclopentadienylmethyl)norborn-5-ene] are dispersed in the matrix by ring opening metathesis polymerisation using W or Mo alkylidene catalysts. Subsequent reduction of the metal complexes in the solid polymer affords the metal particles. The result is the selective concentration of the nanoparticles in selected areas [33].

These organometallic precursors may also be decomposed in harsher conditions. Thus $Pd_2(dba)_2$ is transformed by ultrasound irradiation into agglomerated clusters of ca 80 nm containing nanosized particles. This material was found catalytically active for Heck coupling reaction [34].

1.1.2 Stabilization by Ligands

The decomposition of $Ru(C_8H_{10})(C_8H_{12})$ by dihydrogen (1-3 atm) previously mentioned can occur in the presence of various ligands: long chain thiols or amines, phosphines, oxazolines, alcohols, silanes. In the presence of thiols or amines [26], hcp particles of 2-3 nm mean size form, which display a low size dispersity. The ^1H and ^{13}C NMR spectra of octanethiol protected ruthenium particles point to the absence of exchange between free and coordinated ligands at the NMR time scale. In this case it is possible to observe by ^{13}C NMR the carbon atoms of the alkyl chain of the coordinated ligand as broad peaks except for the carbons located in the α and β positions relative to sulphur which are too broad to be observed.

In the case of the particles accommodating amine ligands, a new phenomenon has been evidenced, namely a dynamic exchange at the NMR time scale between free and coordinated amines. It has been correlated to the TEM and HREM results which show that, at the early stage of the reaction, the particles display a spherical aspect and a small size (ca. 2-3 nm) and that after a few hours the particles coalesce into elongated wormlike particles still constituted of pure, unoxidized hcp ruthenium. This NMR observation is particularly interesting since it evidences for these particles a fluxionality similar to that of molecular clusters which is well documented. The ruthenium nanoparticles contain coordinated mobile surface hydrides as recently demonstrated by a combination of NMR techniques in solution, gas phase and in the solid state [35].

The nature of the stabilizing ligand can be very diverse, for example heptanol and organosilane have recently been used for the stabilization of ruthenium particles. Thus, reaction of $Ru(C_8H_{10})(C_8H_{12})$ with H_2 in heptanol [36], leads to particles of low size dispersity (3 nm), well dispersed in the solvent and adopting the hcp structure of bulk ruthenium. Using octylsilane as stabilizer, the decomposition of $Ru(C_8H_{10})(C_8H_{12})$ under H_2 produces 2.3 nm Ru nanoparticles displaying a narrow size distribution. Infrared spectroscopy and both solution and solid NMR investigations could be successfully applied to characterize the alkysilane fragments grafted on the Ru nanoparticles [37].

Pd nanoparticles were similarly prepared through decomposition of $Pd_2(dba)_3$ under H_2 in the presence of HDA or polyphosphines as stabilizers. The influence of the ligands on the particles shape was established: good ligands like polyphosphines lead to stable spherical nanoparticles of small size (near 2 nm) while the HDA protective effect depends on the ligand concentration as a result of equilibria present at the surface of the particles and monitored by solution NMR spectroscopy [38].

$Pt(dba)_2$ reacts with CO in THF to give a colloid containing fcc particles of 1.2 nm mean size and displaying a narrow size distribution. This colloid is relatively stable and can further be used as a starting material to prepare ligand protected platinum nanoparticles. Addition of 0.2 eq. PPh_3 to this reaction mixture or decomposition of $Pt(dba)_2$ in the same medium in the presence of phosphine leads to phosphine protected particles which adopt a non-periodic icosahedral structure. Interconversion between the two colloids is possible by addition of CO on one side or of PPh_3 on the other. These species are well defined and relatively robust [39]. It may therefore be interesting to emphasize their similarity with the molecular cluster $Pd_{145}(CO)_{60}(PEt_3)_{30}$ recently characterized by Dahl. The size of the metal core of this cluster is estimated to be of the same order of magnitude as these platinum phosphine colloids and it is noteworthy that this Pd_{145} cluster adopts a non-periodic structure [40].

These experimental procedures are not specific of the phosphine ligands and may be employed using more classical ligands for nanoparticles such as octanethiol [31]. In this case, a very stable colloid is formed which may be isolated from the reaction medium and re-dissolved for reactivity or spectroscopic studies. The colloid contains monodisperse fcc particles of 1.6 nm mean size. WAXS studies demonstrate the strong fixation of the ligands at the surface of the particles *(Fig. 3)*. This is corroborated by solution NMR studies that, like for ruthenium, evidence the absence of exchange between free and coordinated ligands at the NMR time scale.

The strong coordination of sulphur to platinum enables the construction of "supramolecular" networks incorporating the metal particles. Thus platinum particles of 1.6 nm mean size can be prepared using as protecting ligands thiophenols substituted in the 4 position by a hydroxo, a carboxylate or an amino group [41]. Self-assembly of the nanoparticles is observed for the colloids stabilized by 4-HO-C_6H_4-SH or

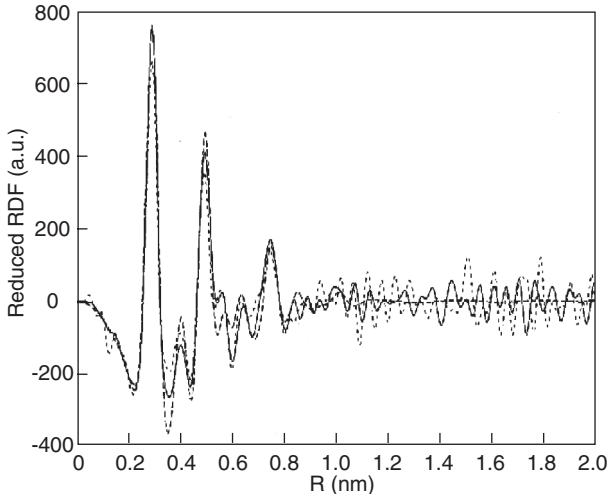

Figure 3

WAXS analysis of octanethiol stabilized Pt colloid (solid line: experimental data; dotted line: cuboctahedral model) (Adapted from Reference 28).

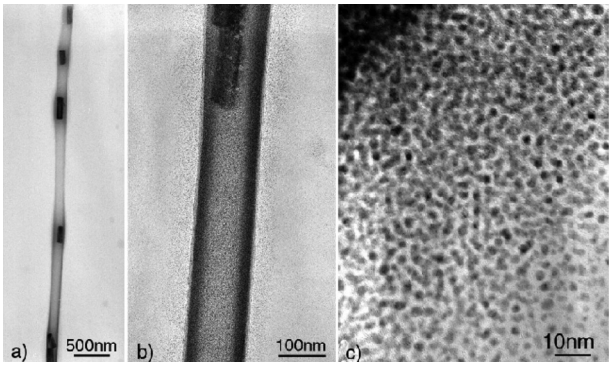

Figure 4

HREM micrographs of nanotubes resulting from the assembly of Pt nanoparticles stabilized by a 1:1 mixture of the 4-HO-C_6H_4-SH and 4-H_2N-C_6H_4-SH (Adapted from Reference 41).

4-HOOC-C_6H_4-SH. If a mixture containing a 1:1 mixture of the 4-HO-C_6H_4-SH and 4-H_2N-C_6H_4-SH is used, the particles self-organize into very long nanotubes the walls of which are constituted by a monolayer of platinum nanoparticles *(Fig. 4)*.

Fluorinated thiols (perfluorooctanethiol, $C_6F_{13}C_2H_4SH$) were also used by Korgel and Johnston to stabilize platinum and iridium nanoparticles prepared in super critical carbon dioxide by hydrogenation of the organometallic precursors $PtMe_2(C_8H_{12})$ and $CpIr(C_8H_{12})$ at 80°C and 276 bar [42]. Pt and Ir nanocrystals are obtained with a mean size comprised between 2 and 12 nm as a function of predominantly the precursor concentration (higher concentrations giving rise to larger particles). The long chain perfluoronated thiol ligands leads to a good solubility of the nanoparticles in the environmentally benign CO_2 solvent.

The synthetic method described hereabove is very simple and can be in principle transposed to any metal/ligand combination. One of the most challenging problems regarding the use of nanoparticles in catalysis concerns asymmetric catalysis. Only a few examples of asymmetric heterogeneous catalysis have been reported, the most popular ones are based on a platinum cinchonidine system [43-45]. Using the chiral xylofuranoside diphosphite ligand Pd nanoparticles with a mean size of 4 nm were synthesized which display a novel activity in enantioselective allylic alkylation of *rac*-3-acetoxy-1,3-diphenyl-1-propene with dimethylmalonate: the reaction proceeds with only one enantiomer of the substrate, hence demonstrating a very high degree of kinetic resolution [46]. Phosphine stabilized palladium nanoparticles were also recently reported by Hyeon et al. through thermolysis of $Pd(acac)_2$. They compared the spectroscopic properties of the nanoparticles to those of molecular complexes prepared by substitution of dba on $Pd(dba)_2$ [47].

Asymmetric oxazolines or amino alcohols provide an excellent stabilization of platinum particles, which can be handled like molecular species. Self-organized superstructures adopting shapes of wires or of pseudo-crystals form spontaneously probably due to ligand interactions through hydrogen bonding [48]. Very small Ruthenium nanoparticles *(Fig. 5)* containing the same ligands (1 to 2 nm according to the ligand) were used in catalytic reactions such as asymmetric hydrogenation or asymmetric hydrogen transfer but so far leading only to poor enantioselectivity [49].

1.1.3 Stabilization by Ionic Liquids

A great attention is presently devoted to efficient catalytic systems that might combine the advantages of both homogeneous (catalyst modulation) and heterogeneous (catalyst recycling) catalysis. Ionic liquids appear as very interesting systems since they can be considered as non-polluting solvents and can also provide facile products separation and catalysts recycling. The group of Dupont has developed for a few years the synthesis of transition metal nanoparticles in room temperature ionic liquids as stabilizers with the objective to test them in hydrogenation or carbon-carbon coupling catalytic reactions. These authors use the same method as that developed in our group, *i.e.* the hydrogenation of organometallic precursors like Ru(cod)(cot), $Pt_2(dba)_3$ or $[Ir(C_8H_{12})Cl]_2$.

Thus, the use of imidazolium ionic liquids allowed the formation and the stabilization of iridium nanoparticles [50].

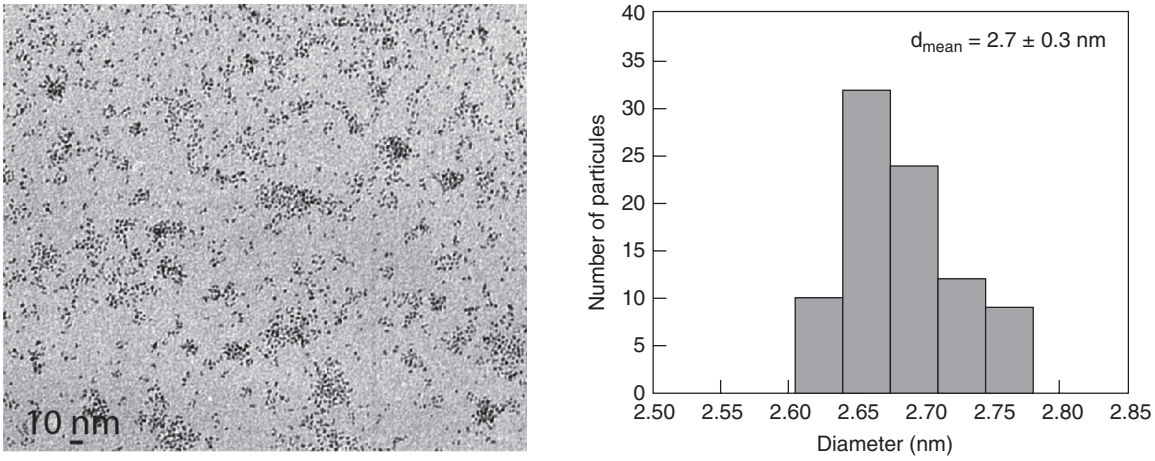

Figure 5

TEM image of oxazoline stabilised ruthenium nanoparticles and corresponding size histogram (mean size = 2.7 nm) (Adapted from Reference 49).

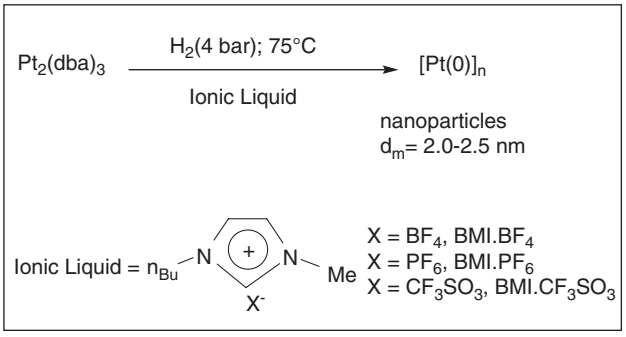

Scheme 2

Synthesis of Pt nanoparticles in ionic liquids (Adapted from Reference 53).

Treatment of the complex $[IrCl(C_8H_{12})_2]_2$ in 1-*n*-butyl-3-methylimidazolium hexafluorophosphate ([BMI][PF6]) under dihydrogen (4 bar) at 75°C affords the formation of a colloidal solution containing well-dispersed Ir nanoparticles with a mean size of 2.5 nm. This solution promoted biphasic hydrogenation of various olefins under mild reaction conditions. The olefin loss with time has been followed under a constant pressure of H_2: sigmoidal curves which could be fitted to the A → B, A + B → 2B autocatalytic mechanism characteristic of nanocluster formation and growth were obtained as previously observed by Finke *et al*. The products could be isolated almost quantitatively by simple decantation, and the isolated Ir nanoparticles maintained their efficiency for up to at least seven recycles. These Ir nanoparticles are also active for arenas [51] and ketones [52] hydrogenation.

The same methodology could be applied to platinum using $Pt_2(dba)_3$ and various room temperature ionic liquids and led to metallic Pt nanoparticles with a mean size near 2.0-2.5 nm *(Scheme 2)* [53]. The isolated Pt(0) nanoparticles could be redispersed in the ionic liquid or in acetone or else used in solventless conditions for liquid-liquid biphasic, homogeneous, or heterogeneous hydrogenation of alkenes and arenes under mild reaction conditions (75°C, 4 bar H_2). Recycling experiments have also been performed.

The use of the complex $Ru(C_8H_{10})(C_8H_{12})$ for the formation of small Ru(0) nanoparticles *(Fig. 6)* dispersed in 1-*n*-butyl-3-methylimidazolium hexafluorophosphate (BMI·PF_6), tetrafluoroborate (BMI·BF_4) or trifluoromethane sulfonate (BMI·CF_3SO_3) has also been described [54]. In this case, small nanoparticles with diameters of 2.6 ± 0.4 nm which were agglomerated inside spherical superstructures (diameters ~57 nm) were obtained, giving rise to efficient multiphase catalytic activity for alkenes and benzene hydrogenation under mild conditions (75°C; 4 bar). When benzene was used as substrate, an interesting partial hydrogenation has been reported leading to the formation of cyclohexene with a selectivity of up to 39% at low benzene conversion.

Very recently, the same authors reported the synthesis of stable ligand-free Pd nanoparticles dispersed in the BMI·PF_6 ionic liquid and displaying an irregular shape with a monomodal particle size distribution centred at 1.7 ± 0.3 nm [55]. Their catalytic properties have been tested in the Heck coupling of aryl halides with *n*-butylacrylate at different temperatures with interesting results. However, TEM investigations revealed changes in shape and in size of colloidal Pd catalysts (mean size after catalysis: 6.01 ± 0.7 nm) and ICP-AS analysis showed significant metal leaching from the ionic phase to the organic one at low substrate conversion. The authors considered that these results were strong indications that Pd nanoparticles dispersed in the ionic liquid act as a reservoir of catalytically active Pd species.

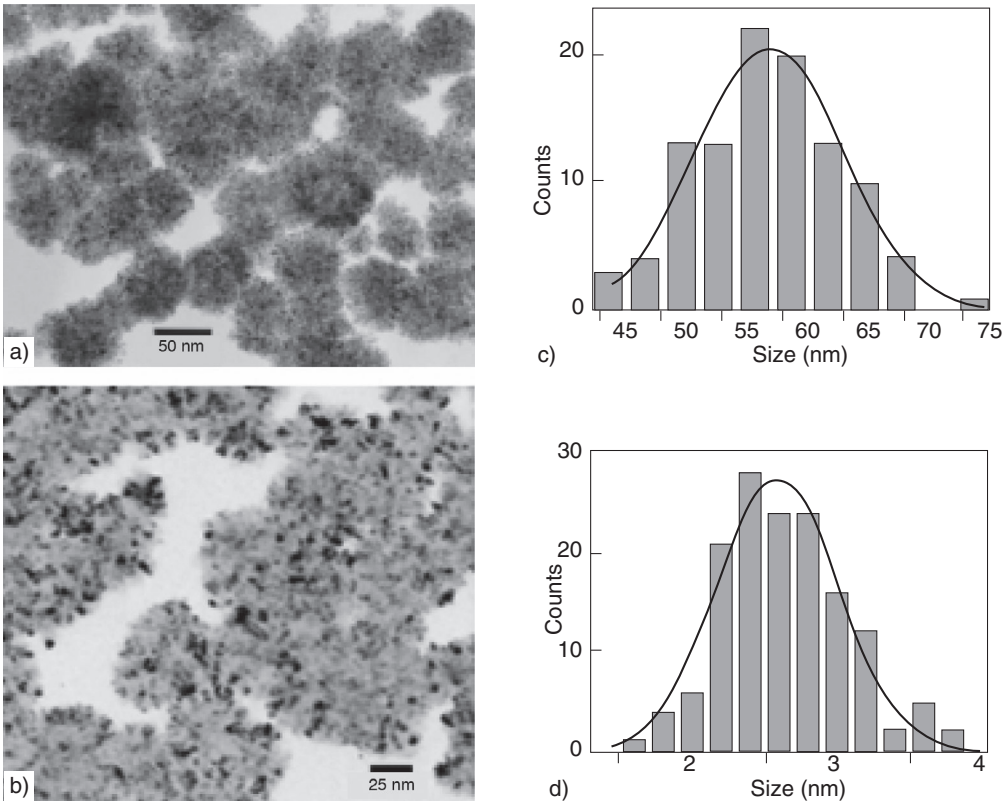

Figure 6

Images of the Ru nanoparticles prepared in BMI·PF_6 showing a) the superstructures, b) inside the spherical superstructures, and the corresponding histograms (c and d) (Reference 54).

1.1.4 Stabilization by the Reaction Medium

When using $Ru(C_8H_{10})(C_8H_{12})$, the decomposition by H_2 in neat THF or in non-coordinating solvents such as pentane leads to the precipitation of ill-defined ruthenium powder. However, when using alcohols as solvents, the reaction produces colloidal solution containing ruthenium particles which are stable for over one year under argon but which precipitate upon exposure to air [56]. The particles prepared in neat methanol are very large, polycrystalline (76 nm), mesoporous and display a relatively large specific area (>40 $m^2 \cdot g^{-1}$). In THF/methanol mixtures, the size of the polycrystalline particles was found to depend upon the reaction medium. It remains of the same order of magnitude as that observed in neat methanol up to a THF content of 25 vol.% after which the size decreases linearly with the THF content: for a THF content in the solution of 50 vol.%, the size of the particles is 47 nm, for 90 vol.% 20 nm and for 97.5 vol.%, ca. 3-6 nm *(Fig. 7)* [57]. A similar trend, namely size decrease, is observed upon changing MeOH for higher alcohols. The size of the particles is *ca.* 5 nm when the reaction is carried out in isopropanol and *ca.* 2.5 nm in pentanol. Finally, it was found for the reactions carried out in MeOH/THF mixtures that addition of cyclooctane leads to an increase in the size of the particles. These surprising results were attributed to phase separation in the solution between cyclooctane resulting from hydrogenation of the ligands of the ruthenium precursor and the alcohol. In this respect, the larger droplets would be formed in the most polar solvent systems and hence the most segregated medium. This is in excellent agreement with the sizes of the particles measured in neat alcohols. The most lipophilic one (pentanol) gives rise to the smallest particles.

The hydrido complex $[(1,5\text{-}C_8H_{12})RhH]_4$ can be used as a source of small rhodium crystallites. Aromatic hydrocarbon solutions of this complex are unstable when exposed to dihydrogen, allowing the formation of 2 nm size, crystalline but agglomerated Rh nanoparticles that show catalytic properties in arene hydrogenation [58].

1.2 Organometallic Synthesis of Magnetic Metal Nanoparticles

1.2.1 Stabilization by Polymers

In a way very similar to $Ru(C_8H_{10})(C_8H_{12})$, the complex $Co(C_8H_{13})(C_8H_{12})$ readily decomposes at room temperature in solution in the presence of a low pressure (generally 3 bars) of dihydrogen. When using PVP as a stabilizer,

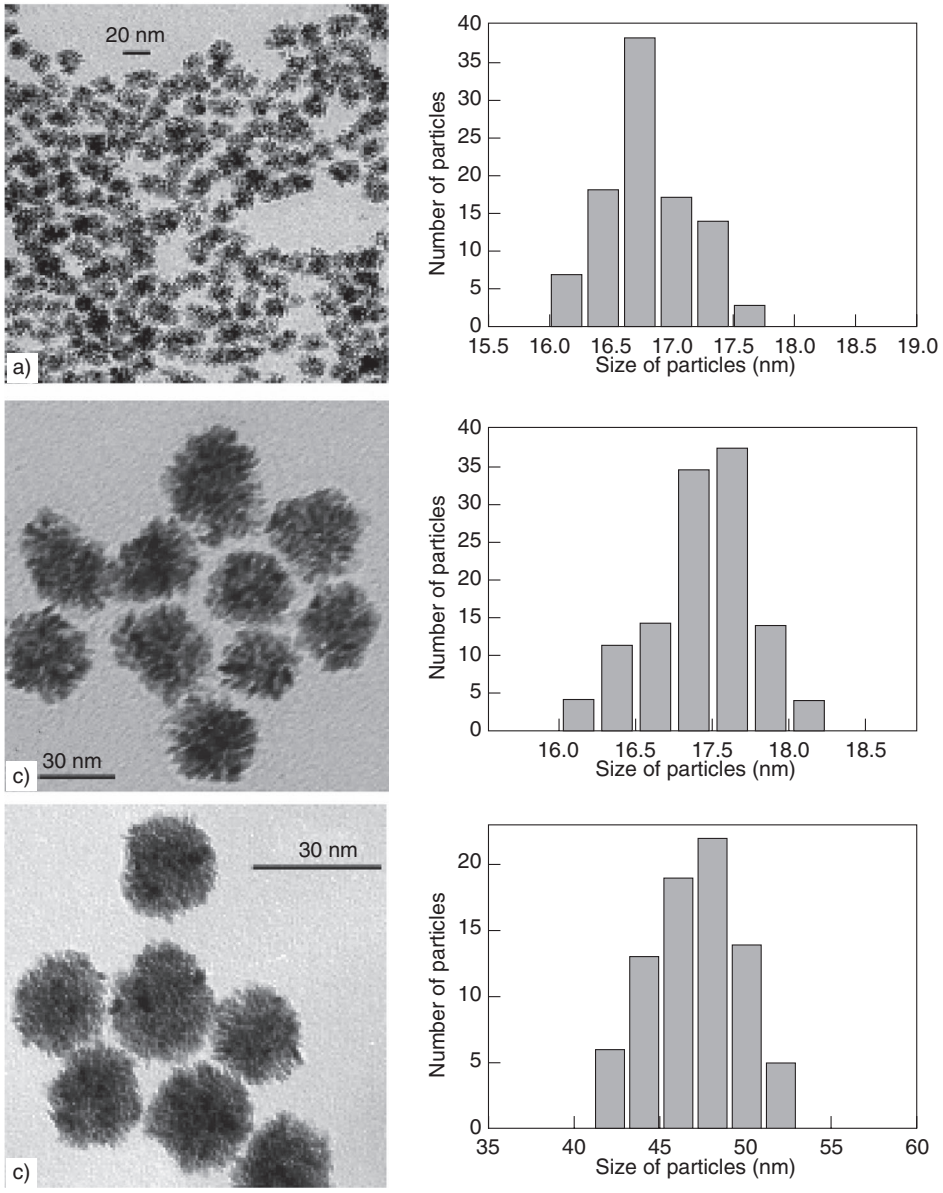

Figure 7

Micrographs and size histograms of Ru nanoparticles synthesized in MeOH/THF mixtures a) MeOH/THF = 5/95; b) MeOH/THF = 25/75; c) MeOH/THF = 50/50) (Adapted from Reference 57).

nanoparticles of 1.6 or 2.0 nm mean size were obtained as a function of the precursor concentration whereas with PPO larger particles (4 nm) form [59]. The particles of small size (1.6 or 2 nm) adopt a non-periodic polytetrahedral structure whereas the larger ones (4 nm) adopt the hcp structure of bulk cobalt [60]. Interestingly, and somewhat surprisingly, these particles were demonstrated to display the same magnetic properties as particles of same size prepared in ultra high vacuum in the gas phase by time-of-flight experiments [61]. Thus the particles are superparamagnetic with blocking temperatures near 10 K and display an enhanced magnetization at saturation per cobalt atom compared to bulk cobalt [62]. Addition of O_2, pyridine, isocyanides or CO leads to a dramatic decrease of the magnetic properties of the particles. This demonstrates:

– the absence or low contamination of the as prepared particles and,
– the presence of a relation between the π-accepting properties of the ligand and the magnetic properties of the nanomaterials.

Nickel particles can be prepared directly by decomposition of $Ni(C_8H_{12})_2$ in dichloromethane in the presence of

polyvinylpyrrolidone: 2 nm or 3 nm particles can be obtained depending on the concentration of the precursor [63]. The particles adsorb CO in solution in both bridged and linear geometries. Vibrational couplings between adsorbed CO molecules were detected, consistent with an ordered surface for the colloidal nickel particles.

Nickel particles may also be prepared by decomposition of the same precursor, $Ni(C_8H_{12})_2$, by H_2 in THF or a hydrocarbon solvent. The particles display a larger size (4-5 nm) and adopt the fcc structure of bulk nickel. These particles present the same magnetic properties as bulk nickel [64]. Coordination studies at their surface confirm the strong magnetization decrease in the presence of CO but also demonstrate that coordination of a pure σ-donor ligand such as amines has no effect on the magnetic properties of the particles [65].

As for noble metal particles, this synthetic method can be adapted to the preparation of bimetallic nanoparticles. Thus Co-Pt, Co-Rh and Co-Ru particles [66-68] of various compositions have been prepared by co-decomposition of $Co(C_8H_{13})(C_8H_{12})$ with $Pt(dba)_2$, $Rh(acac)(C_8H_{12})$ or $Ru(C_8H_{10})(C_8H_{12})$. As a general rule, nanoparticles of size found between 1.5 and 2.5 nm were obtained whatever the metals and the compositions. Platinum metals rich nanoparticles adopt the structure of the corresponding metal, namely fcc, fcc and hcp whereas cobalt rich particles adopt the polytetrahedral structure of cobalt. For intermediate compositions, as yet unknown non-periodic structures are observed. The bimetallic nanoparticles show an enhanced coercivity as compared to cobalt in agreement with an enhanced anisotropy as also observed in bulk alloys.

1.2.2 Stabilization by Ligands

The stabilization of magnetic nanoparticles can also be achieved by ligands or ligand mixtures. The decomposition of $Co(C_8H_{13})(C_8H_{12})$ in the presence of long chain acid and/or amine ligands yields nanoparticles of controllable size, shape and therefore magnetic properties [69]. Thus, decomposition of $Co(C_8H_{13})(C_8H_{12})$ in the presence of a mixture of oleic amine and oleic acid affords at room temperature spherical nanoparticles of ca. 4 nm mean size. However at 150°C in the presence of dihydrogen, these particles convert into regular nanorods. Changing the length of the hydrocarbyl chain of the amine surprisingly allows the control of the aspect ratio of the rods from *ca.* 1.5 for octylamine to ca. 25 for hexadecylamine *(Fig. 8)* [69]. Upon changing the shape and the aspect ratio of the nanoparticles, it is also possible to control the magnetic properties of the nano-objects from superparamagnetic to ferromagnetic at room temperature. An appropriate choice of a long alkyl chains ligands mixture (hexadecylamine/stearic acid) leads to the formation of unprecedented hexagonal superlattices of nanorods resulting from crystallization in solution *(Fig. 9)* [70].

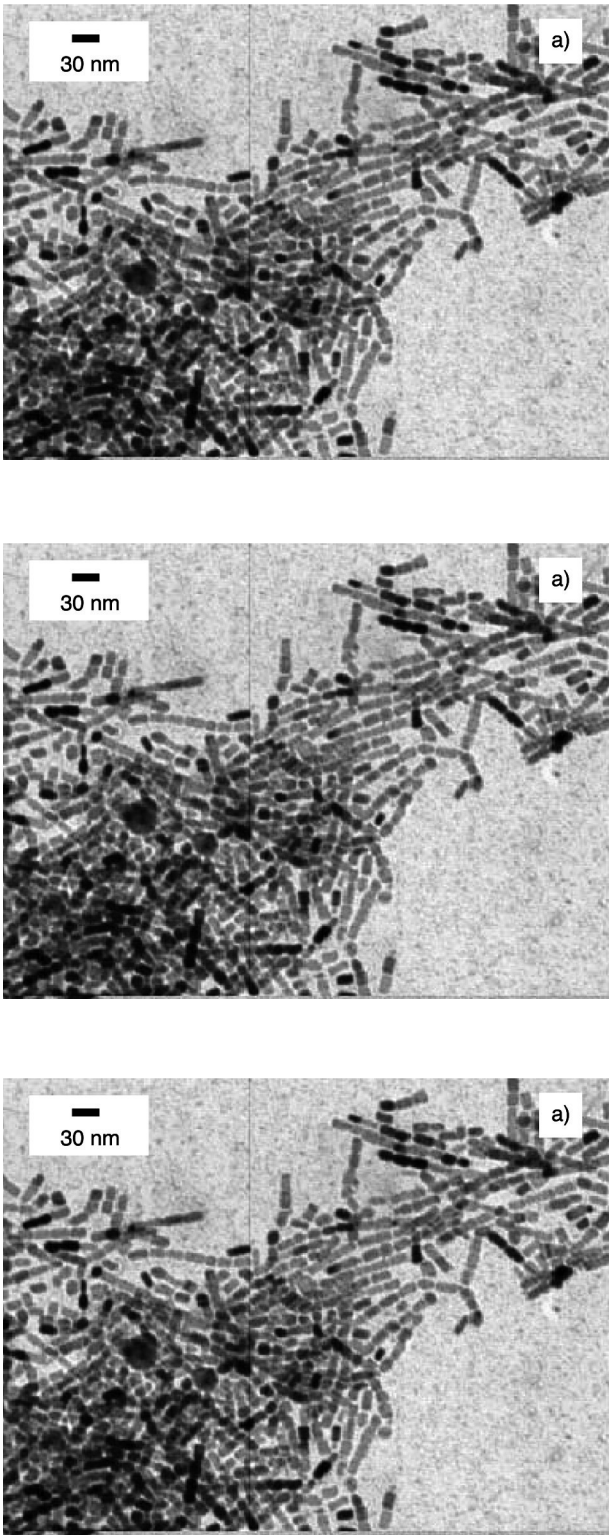

Figure 8

TEM micrographs of amine stabilized cobalt nanoparticles a) C_8NH_2; b) $C_{12}NH_2$; c) $C_{16}NH_2$ showing the variation of the aspect ratio according to the length of the amine alkylchain (Adapted from Reference 69).

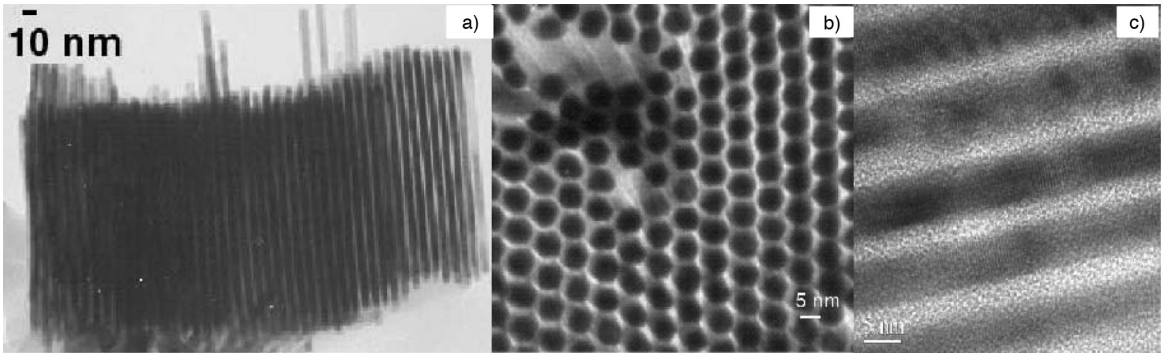

Figure 9

TEM a) and b) and HREM c) micrographs of self-organized Co nanorods stabilized by a stearic acid/hexadecylamine mixture (Adapted from Reference 70).

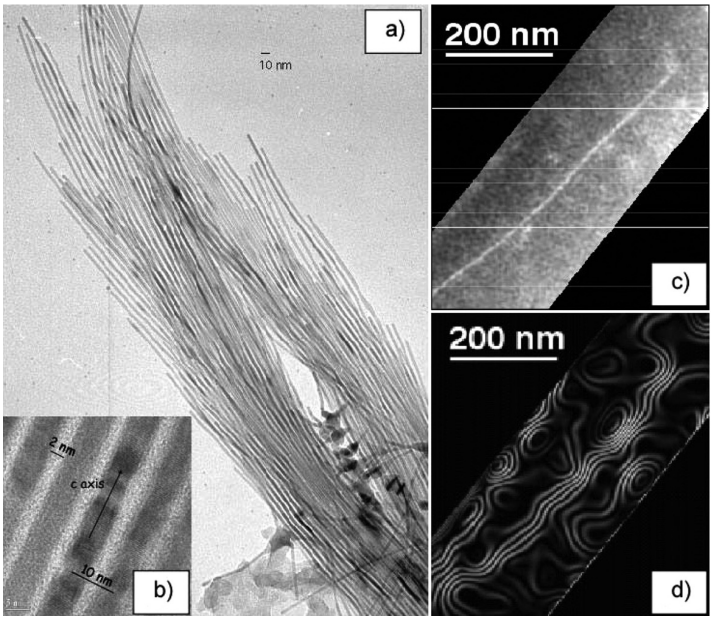

Figure 10

TEM a) and HREM b) and holography c) and d) images of Co nanowires (Adapted from Reference 71).

The ratio of the different component of the ligand mixture also dramatically influences the shape of the particles. Thus, in the presence of oleic acid only, the reaction of decomposition of $Co(C_8H_{13})(C_8H_{12})$ produces very regular spherical nanoparticles which form super-lattices in 2 or 3 dimensions upon deposition over a carbon grid whereas using a 2:1 mixture of oleic acid and oleylamine leads to the formation of very long Co nanowires of 4 nm mean diameter and exhibiting the same hcp structure as the nanorods and bulk cobalt. It has recently been possible using magnetic holography to measure the magnetic properties of one such nanowire *(Fig. 10)*. In all cases, the nano-objects display a magnetization at saturation per cobalt atom identical to that observed for bulk cobalt, hence demonstrating the absence of influence of pure σ-donor ligands such as amines and acids on their magnetic properties [71].

In the case of iron, the decomposition of the $Fe[N(SiMe_3)_2]_2$ complex in the presence of a long-chain acid and a long-chain amine mixture in various proportions produces monodisperse zerovalent iron nanoparticles displaying magnetic properties that match those of bulk iron. These nanoparticles adopt a cubic shape and are incorporated into extended crystalline superlattices containing nanocubes in close proximity and with their crystallographic axes aligned *(Fig. 11)* [72].

Similar reactions were carried out with nickel using $Ni(C_8H_{12})_2$ as a precursor but in the presence of amines only. It was found that the relative concentrations of amine and nickel are decisive as far as the aspect ratio of the particles is concerned. For a low concentration of amine spherical particles or double-arrow shaped particles were obtained whereas for 10 eq. of amine relative to nickel very regular nanorods

of *ca*. 3 nm mean diameter were formed. Again, all these species display the same magnetization at saturation as bulk nickel. This contrasts with particles produced in the presence of TOPO as ligands which show a reduced magnetization which was attributed to the π-accepting properties of the ligand [73].

Bimetallic NiFe and CoFe nanoparticles were prepared by associating an olefinic complex, $Ni(C_8H_{12})_2$ or $Co(C_8H_{13})(C_8H_{12})$ to $Fe(CO)_5$. NiFe particles were synthesized in the presence of HDA in refluxing anisole. The particles are monodisperse, display a size of 3.3 nm and organize into 2D and 3D super-structures on a carbon grid [74]. In similar conditions but in the presence of long chain amines and long chain acids, the reaction between $Co(C_8H_{13})(C_8H_{12})$ and $Fe(CO)_5$ affords in excellent yield a black crystalline material which precipitates from the solution. As shown in Figure 12, the super-crystals of millimetric size are composed of monodisperse nanoparticles organized into a

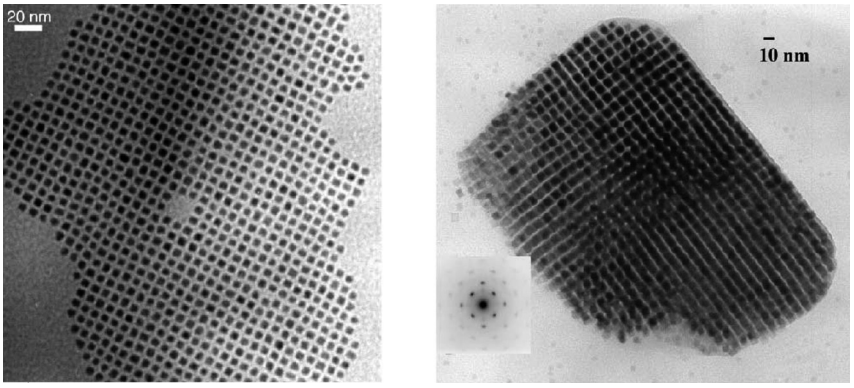

Figure 11

Cubic shape iron nanoparticles self-assembled into cubic extended crystalline superlattices (Adapted from Reference 72).

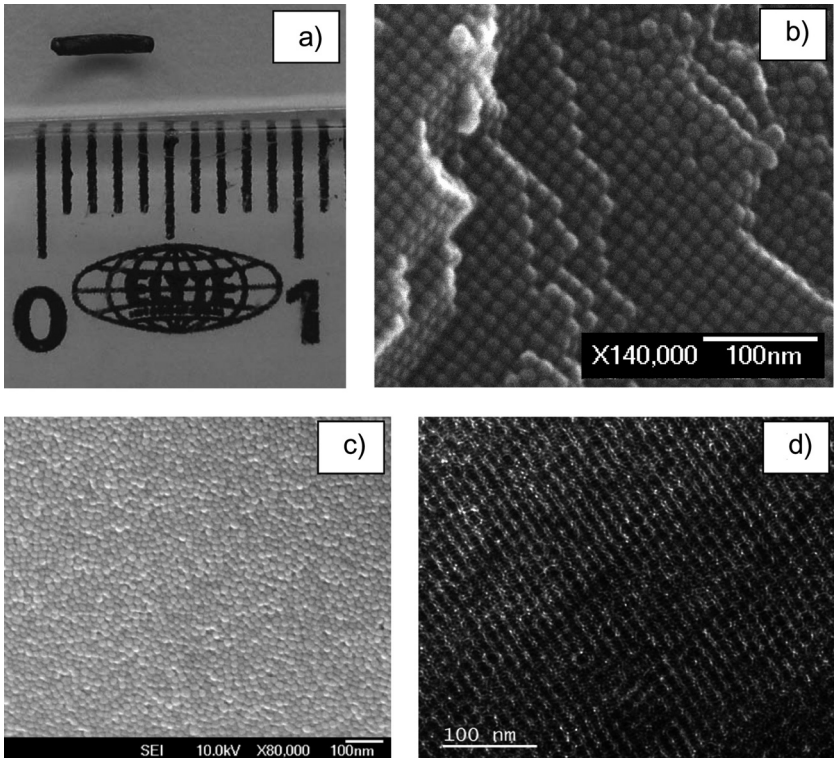

Figure 12

a) Image of a FeCo super-crystal of the millimetric size; b) SEM-FEG image of a FeCo super-crystal; c) SEM-FEG image of the surface of a FeCo super-crystal; d) TEM-FEG image after ultramicrotomy of a FeCo super-crystal (Adapted from Reference 75).

compact super-lattice shown on a broken super-crystal to be fcc. These particles display interesting soft magnetic properties but slowly oxidize in air. A thermal treatment of the super-crystals at 500°C for 30 minutes allows the deposition on the surface of the individual particles of a thin graphite layer. Before annealing the particles adopt a polytetrahedral structure which transforms into bcc like bulk Fe-Co after annealing [75].

1.3 Organometallic Synthesis of Nanoparticles of Other Metals and Main Group Elements

1.3.1 Metals

The organometallic approach can bee extended to d^{10} metals and to main group elements. For example, CpCu(^{t}BuNC) is decomposed by CO at room temperature to give copper nanoparticles which may be stabilized by polymers (PVP, PPO) [76] or by PPh_3 [77]. Although not an organometallic complex *stricto sensu*, the alkoxide $Cu(OCH(Me)CH_2NMe_2)_2$, known to be a CVD precursor, can be used to produce copper nanoparticles upon thermolysis at 300°C in HDA. The particles have a size of ca. 7.5 nm and a strong tendency to organize into 2-D super-lattices [78].

The dialkyl $ZnCy_2$ complex (with Cy = η^1-C_6H_{11}) decomposes thermally at 130°C in wet anisole to produce 6 nm Zn particles protected by a thin ZnO layer. Full oxidation of the particles at 600°C leads to ZnO particles of similar size and geometry [79]. Upon mixing a dialkylzinc, namely $ZnEt_2$ and $Cu(OCH(Me)CH_2NMe_2)_2$ in HDA at 250°C, it is possible to prepare bimetallic Cu/Zn particles of various relative composition and of mean size between 5 and 10 nm. EDX and SAED (selected area electron diffraction) demonstrate the presence of the CuZn and $CuZn_2$ besides Cu, hence demonstrating the alloying of copper and zinc *(Fig. 13)* [80].

The decomposition of CpIn whether thermal or photochemical rapidly produces In(0) nanoparticles [81]. When the reaction is carried out using PVP as a stabilizer, the presence of a small amount of water is required in order to obtain monodisperse indium nanoparticles. In the presence of the oxygen donor ligand TOPO, the decomposition of a toluene solution of CpIn produces rigorously monodisperse 5 nm In particles which self-assemble into a hcp super-lattice *(Fig. 14a, b)*. In the same conditions but using HDA instead of TOPO, slightly elongated particles were obtained which did not show any sign of self-organization [82]. In this case, the rate of decomposition was also found important since the same reaction carried out in the presence of UV light yields very long (mm) indium nanowires, the diameter of which can be adjusted to some extent by the concentration of HDA present in the solution. This procedure can be adapted to the production of In_3Sn nano-ribbons upon using a mixture of CpIn and $[Sn(NMe_2)_2]_2$ as precursors *(Fig. 14c)*. Finally CpIn also decomposes spontaneously in methanol at room temperature

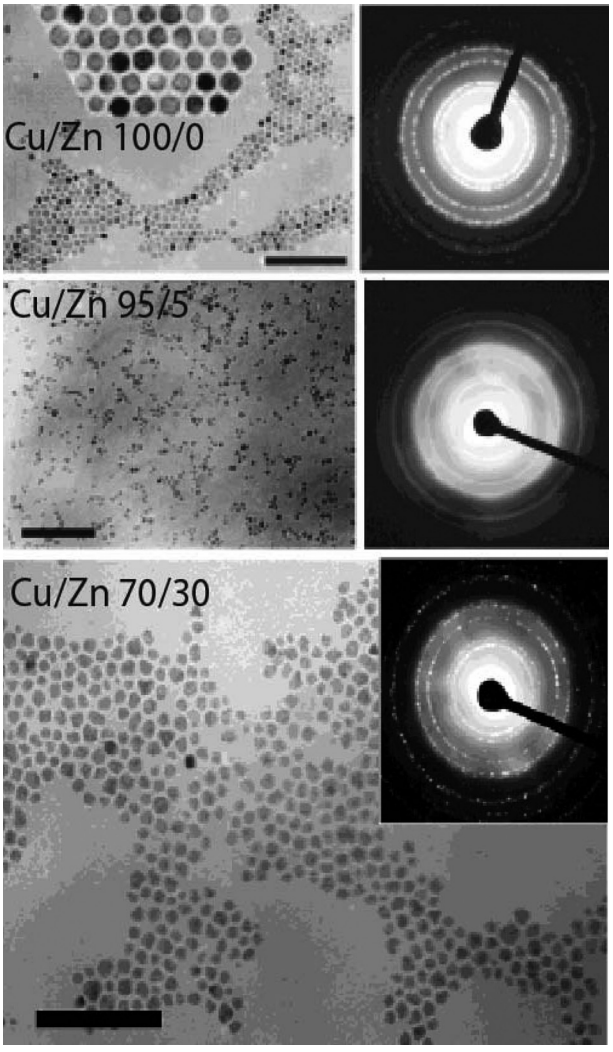

Figure 13

TEM images and SAED (selected area electron diffraction) of the toluene solutions of Cu/Zn 100/0 (scale bar = 110 nm), 95/5 (scale bar = 175 nm) and 70/30 (scale bar = 116 nm) systems stabilized in hexadecylamine (Adapted from Reference 80).

to give aggregates of nanoparticles. The individual particles display a size of *ca.* 15 nm and are included in aggregates of *ca.* 400 nm. These particles may be used for the realization of gas sensors on a silicon chip [83].

$[Sn(NMe_2)_2]_2$ decomposes in toluene under UV irradiation in the presence of HDA and hexadecylammonium chloride (HDA,HCl) in a 3:1 ratio, to form a precipitate which consists of identical ovoid tin particles of 18 × 15 nm [84]. These particles display the tetragonal structure of bulk Sn and are arranged into a non-compact, probably monoclinic 3D super-lattice inside which the atomic planes of individual particles are aligned. The decomposition of $[Sn(NMe_2)_2]_2$ can also be achieved thermally in wet anisole. The quantity

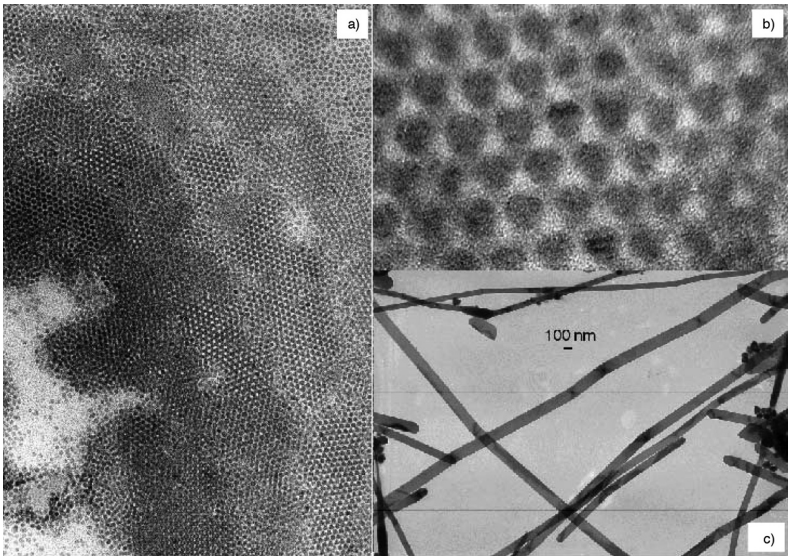

Figure 14

TEM a) and HRTEM b) images of self-organized TOPO-stabilized In nanoparticles synthesized by decomposition of InCp in toluene (individual mean size = 5 nm); c) In_3Sn nanowires obtained by simultaneaous decomposition of toluene solution of InCp and $[Sn(NMe_2)_2]_2$ under UV light in the presence of HDA with the ratio 1/1/0.5 (Adapted from References 81 and 82).

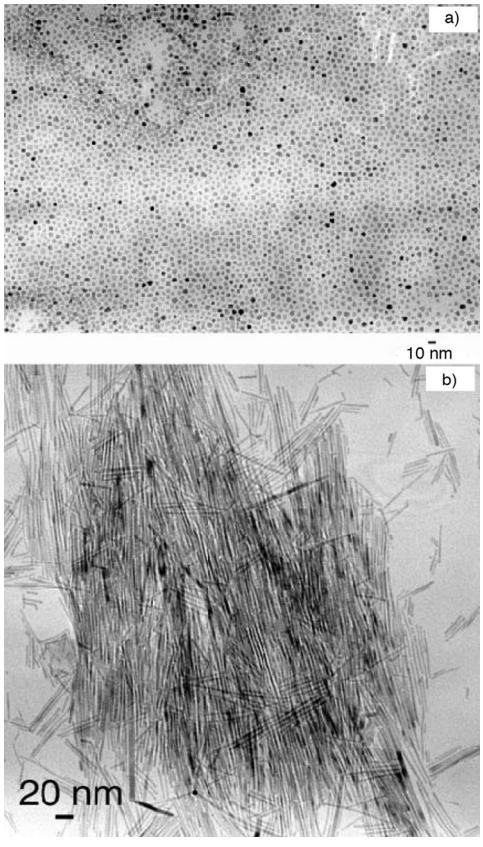

Figure 15

TEM micrographs of ZnO nanodisks obtained by a slow oxidation/evaporation process from a THF solution of HDA a) and ZnO nanowires grown in pure octylamine b) (Adapted from Reference 90).

of water is critical to control the size dispersity of the particles, the optimum being obtained for $[H_2O]/[Sn] = 0.5$. The particles can be oxidized in an oven at 600°C into SnO_2 without changes in their size and shape [85]. They can also be deposited onto the silicon platform of a microelectronic device and oxidized in air using the integrated heater of the chip. In the latter case, the nanomaterial obtained can be used as the sensitive layer of a gas-sensing device [86].

1.3.2 Metal Oxides

Organometallic precursors may also be used for the direct preparation of metal oxide nanoparticles.

As a first example, the organometallic precursor bis(toluene) titanium gave interesting results. Thus, the impregnation of mesoporous alumina by a solution of bis(toluene) titanium leads to a black metallic deposit which, after oxidation at 400°C, leads to the growth of TiO_2 nanoparticles [87]. In organic solution bis(cyclooctatetraene) titanium complex ($Ti(C_8H_8)_2$) reacts with dry DMSO to yield a precipitate of amorphous TiO_2. In the presence of phosphorus ligands, namely PBu_3, $OPBu_3$ and $OPOct_3$, crystalline nanoparticles in 3-25 nm range can be obtained, depending upon the ligands [88].

Zinc alkyl derivatives have been widely used for the preparation of ZnO nanoparticles. Thus, decomposition of $ZnEt_2$ in the presence of O_2 at high temperature (200°C) in TOPO produces TOPO capped ZnO nanoparticles [89].

The decomposition of the dialkylzinc precursor ($ZnCy_2$) can be carried out at room temperature in the presence of H_2O vapour and various ligands. In this case, crystalline and luminescent nanoparticles adopting the zincite phase are

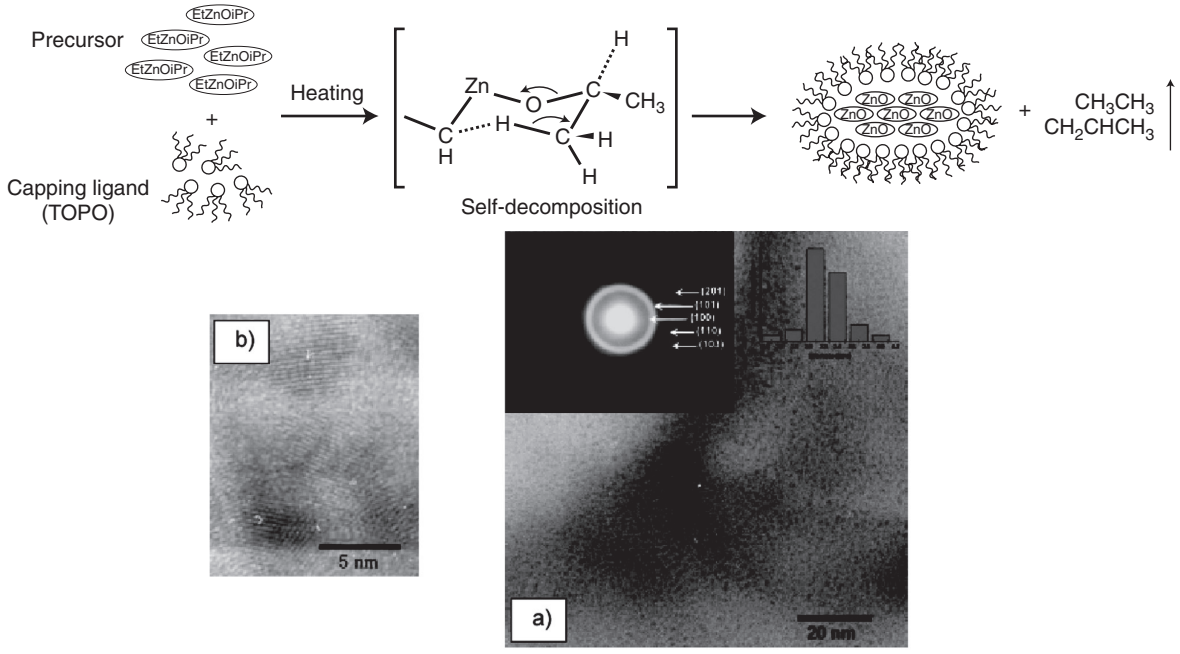

Figure 16

Schematic thermolysis of EtZnOiPr precursor in the presence of TOPO and TEM a) and HREM b) images of the so-obtained ZnO nanoparticles (Adapted from Reference 93).

produced [90]. The size and shape of the particles can be modulated, depending upon the nature and concentration of the amine ligand used, from spherical particles in the 3-4 nm range to very long (>100 nm) nanorods of 4 nm diameter *(Fig. 15)*. It is demonstrated by NMR that the ligand coordinates on the zinc precursor as well as on the oxide nanoparticles and therefore is probably present throughout the oxidation process [91]. The same reaction carried out using a mixture of long chain amines and long chain carboxylic acids as stabilizers produces monodisperse spherical nanoparticles in the 3-4 nm range which self-organize into 2-D or 3-D super-lattices depending upon the nature of the ligands [92]. ZnO nanoparticles can also be produced by thermolysis of $EtZnO^iPr$ at 160°C in TOPO without the need for any extra oxygen source. In this case, 3 nm crystalline hexagonal particles are obtained *(Fig. 16)* [93].

2 INCLUSION OF METAL NANOPARTICLES INTO TEMPLATES

The organometallic approach for the synthesis of nanoparticles of metals or metal oxides can also be applied for the preparation of composite materials. Some results have been obtained using alumina membranes or mesoporous silica as templates for the inclusion of metal nanoparticles. Metal oxide nanoparticles could also be obtained in these conditions after a calcination step under air of pre-formed metal nanoparticles without change in size and dispersion of the nanoparticles.

2.1 Alumina Membranes

The filling of nanoporous alumina membranes of various pore widths has been carried out from the Ru(cod)(cot) precursor, following two different ways [94]. The first approach involved the use of pre-formed colloidal solutions obtained through decomposition of Ru(cod)(cot) complex in MeOH/THF mixtures, leading to Ru nanoparticles of different sizes depending on the MeOH/THF ratio. Concentrated pre-prepared nanoparticles solutions were transferred into membranes of adequate pore sizes by vacuum induction. In these conditions, only very few agglomerates have been seen outside of the pores, but dense areas were observed within the membrane channels. In addition, it appeared that the difference between the diameter of the pores and the size of the particles has to reach a certain value for the particles to enter the pores, since for instance 20 nm particles do not enter into 25 nm pores. The second approach consisted in the decomposition of Ru(cod)(cot) under usual conditions after deposition of the complex inside the pores using concentrated solutions and vacuum drying. In this way, homogeneous materials displaying well-dispersed and well separated Ru nanoparticles were obtained in the pores of alumina membranes *(Fig. 17)*. The size of the particles was dependent on the pore diameter of the template.

Some of these materials have been tested in the catalytic hydrogenation reaction of 1,3-butadiene in the gas phase giving rise to interesting results showing an increasing activity with a decrease of the particles size, as expected for such

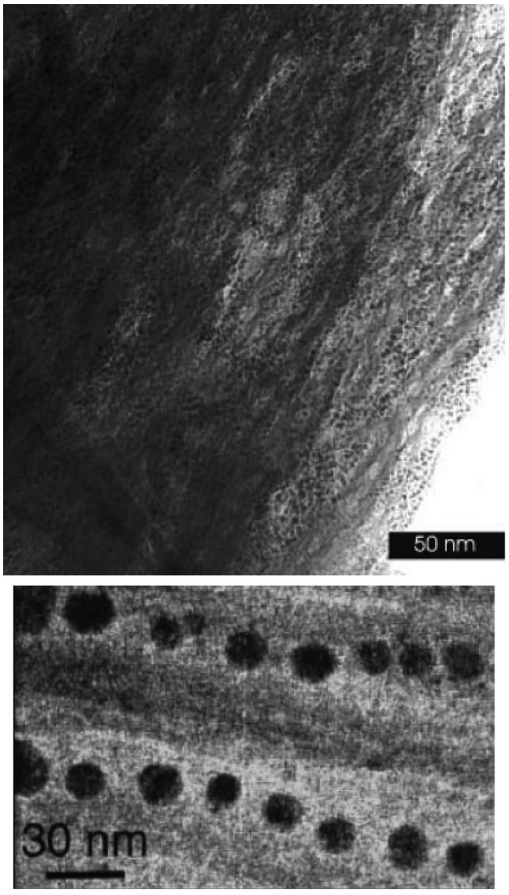

Figure 17

Ru nanoparticles within the channels of alumina membrane.

catalysts. In the same manner, 3 nm Ru nanoparticles synthesized inside alumina membranes were used as catalysts for gas phase oxidation of CO [95]. A trend to higher activities with decreasing particle sizes could be observed.

2.2 Mesoporous Materials

The regular channels of mesostructured porous silica of MCM 41 type have been used as both host and stabilizer for the synthesis of Ru nanoparticles from the organometallic Ru(cod)(cot) precursor following the mild conditions usually used in solution [96]. It appeared clearly that the size of the Ru nanoparticles and their location significantly depend on the mesopore size. For instance, well-dispersed Ru nanoparticles of 3 nm mean size were formed inside 5-8 nm pores of mesostructured silica materials.

Using a two-step procedure based on anchoring an organogold precursor within the channels of functionalized ordered mesoporous silica containing mercaptopropyl groups followed by chemical reduction, composite materials containing gold(0) nanoparticles exclusively within the pore channels could be prepared [97, 98]. Functionalized SBA-15 and HMS-C16 type materials have been used for controlling the growth of gold(0) nanoparticles from $HAuCl_4$ and AuCl(THT). The growth of the particles could be achieved thanks to the thiol functions present in the pores of the silica materials first allowing the anchoring of the metal precursor and secondly retaining the nanoparticles inside the channels of the templates *(Fig. 18)*. It has been shown that the amount of gold incorporated within the materials is linked to the amount of mercapto functions.

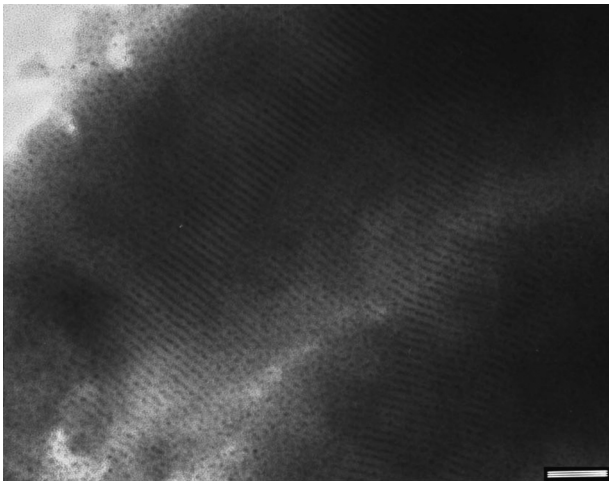

Figure 18

Au nanoparticles within the channels of thiol functionalised ordered mesoporous silica (scale bar = 50 nm).

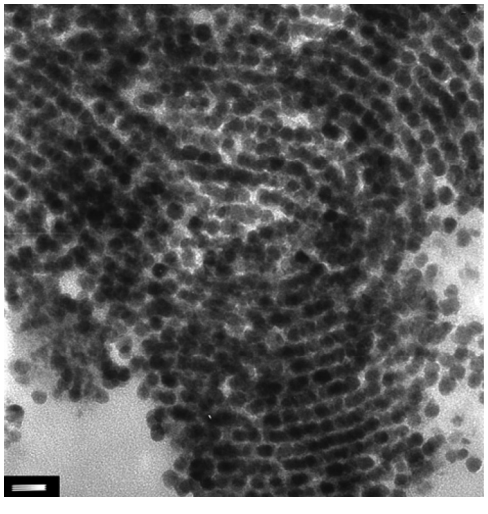

Figure 19

In nanoparticles within the channels of phosphonate functionalised ordered mesoporous silica (scale bar = 20 nm).

Organized mesoporous silica materials containing phosphonate groups have been used for controlling the growth of indium(0) nanoparticles or nanorods, from InCp precursor which decomposes spontaneously at room temperature [99]. The phosphonate groups present in the pores of the solid act as ligands for the coordination of the metal complex and as a stabilizer for the nanoparticles allowing their organization in the channels of the host material *(Fig. 19)*. These In nanoparticles could be further converted to indium oxide nanoparticles after treatment under dioxygen at 200°C without modification of their size and shape. Finally, by modifying the experimental conditions that is, operating at reflux in toluene instead of room temperature, indium nanorods could be obtained and treated in the same way to give indium oxide nanorods.

The same phosphonate functionalised mesoporous silica materials have been recently used as a host for the synthesis of Ru nanoparticles through complexation of Ru(cod)(cot) and further decomposition under usual conditions. Well-dispersed nanoparticles could be obtained in the silica matrix giving rise to hybrid materials displaying an interesting behaviour as catalytic filters to enhance the selectivity of gas sensors [100].

2.3 Synthesis of Composite Materials in a Fluidized Bed

The organometallic approach for the synthesis of metal nanoparticles has been applied to the preparation of hybrid nanocomposites at a high scale using a fluidised bed as reactor [101]. The principle of the technique consists in the spraying of a solution containing an organometallic precursor into a hot fluidised bed of porous fine particles as chosen support. The adequate choice of operating conditions makes possible an uniform deposit of the metal precursor inside the porous matrix. The decomposition of the metal precursor can be realized in the same reactor in mild conditions, giving then rise to hybrid materials containing metal nanoparticles with well-controlled size and composition at a scale at least equal at 30 g of solid. The metal content of the solid can be tuned by an adequate duration of the metallic solution spraying.

CONCLUSION

The use of nano-objects for more and more sophisticated applications has rapidly grown for the past few years. This concerns the fields of catalysis, energy conversion, micro- and nano-electronics, magnetic and optical devices, sensors, biology and more. These applications require in turn complex nanoparticles with size, shape, composition, outer layer and surface species as well controlled as possible. The organometallic approach towards such materials seems perfectly adapted since it allows playing on key synthesis parameters of these very difficult syntheses, namely rate of nucleation, rate of growth and control of the surface chemistry. In particular the surface chemistry may allow both to build complex nanostructures through various associations of surface ligands and leads to a rich surface reactivity involving multiple or cascade reactions. Some spectacular results have been already obtained thanks to this approach but more generally, these elements suggest that there is a strong potential for organometallic chemists to play a key role in this field. This should also lead to an impressive development in surface organometallic chemistry in the future.

REFERENCES

1 Schmid G. (2004) *Clusters and colloids,* from theory to applications, Wiley-VCH, Weinheim, 1994 and Nanoparticles, from theory to applications, Schmid G. (Ed.), Wiley-VCH, Weinheim.

2 de Jongh L.G (1994) *Physics and Chemistry of Metal Cluster Compounds,* Kluwer, Dordrecht.

3 Klabunde K.J., Cardenas-Trivino G. (1996) *Active Metals: Preparation, Characterization, Applications,* Wiley-VCH, Weinheim, pp. 237-277.

4 Lewis L.N. (1998) *Catalysis by Di-and Polynuclear Metal Cluster*, Wiley-VCH Inc., New-York, Weinheim, pp. 373-394.

5 *Metal Nanoparticles*, Feldheim D.L. Foss C.A. Jr (Eds.), Marcel Dekker, New York, 2002.

6 El-Sayed M.A. (2001) *Acc. Chem. Res.* **34**, 257-264.

7 Roucoux A., Schulz J., Patin H. (2002) *Chem. Rev.* **102**, 3757-3778.

8 Cushing B.L., Kolesnichenko V.L., O'Connor C.J. (2004) *Chem. Rev.* **104**, 3893-3946.

9 Katz E., Willner I. (2004) *Angew. Chem. Int. Edit.* **43**, 6042-6108.

10 Müller A., Beckmann E., Bögge H., Schmidtmann M., Dress A. (2002) *Angew. Chem. Int. Edit.* **41**, 1162-1167.

11 Marvaud V., Decroix C., Scuiller A., Tuyèras F., Guyard-Duhayon C., Vaissermann J., Marrot J., Gonnet F., Verdaguer M. (2003) *Chem. Eur. J.* **8**, 1692-1705.

12 Hirai H. (1979) *J. Macromol. Sci. Chem.,* **5**, 633-649.

13 Bönnemann H., Braun G., Brijoux W., Brinkmann R., Schulze Tilling A., Seevogel K., Siepen K. (1996) *J. Organomet. Chem.* **520**, 143-162.

14 Yu W., Liu M., Liu H., Ma, X., Liu Z. (1998) *J. Colloid and Interface Sci.* **208,** 439-444.

15 Liu M., Yu W., Liu H. (1999) *J. Mol. Catal. A: Chemical* **138**, 295-303.

16 Pileni M.P. (1993) *J. Phys. Chem.* **97**, 6961-6973.

17 Pileni M.P. (2002) *Metal Nanoparticles*, Marcel Dekker, New York, Chap. 9, pp. 207-236.

18 Philippot K., Chaudret B. (2003) *C.R. Chimie* **6**, 1019-1034.

19 Chaudret B. (2005) *C.R. Phys.* **6**, 117-131.

20 Green M. (2005) *Chem. Commun.* 3002-3011.

21 For selected publications see: Hess P.H., Parker P.H. Jr (1966) *J. Appl. Polym. Sci.* **10**, 1915-1927; Dinega D.P., Bawendi M.G. (1999) *Angew. Chem. Int. Edit.* **38**, 1788-1791; Sun S., Murray C.B. (1999) *J. Appl. Phys.* **85**, 4325-

4330; Puntes V.F., Krishnan K.M., Alivisatos A.P. (2001) *Science* **291**, 2115-2117; Kim S.W., Son S.U., Lee S.S., Hyeon T., Chung Y.K. (2001) *Chem. Commun.*, 2212-2213; Sun S., Murray C.B., Weller D., Folks L., Moser A. (2000) *Science* **287**, 1989-1992; Salgeirino-Maceira V., Liz-Marsan L.M., Farle M. (2004) *Langmuir* **20**, 6946-6950; Park J.I., Cheon J. (2001) *J. Am. Chem. Soc.* **123**, 5743-5746.

22 Duteil A., Quéau R., Chaudret B., Mazel R., Roucau C. (1992) *Chem. Mater.* **5**, 341-347.

23 Pan C., Pelzer K., Philippot K., Chaudret B., Dassenoy F., Lecante P., Casanove M.-J. (2001) *J. Am. Chem. Soc.* **123**, 7584-7593.

24 Bradley J.S., Hill E.W., Behal S., Klein C., Chaudret B., Duteil A. (1992) *Chem. Mater.* **4**, 1234-1239.

25 Duteil A., Quéau R., Chaudret B., Mazel R., Roucau C., Bradley J.S. (1993) *Chem. Mater.* **5**, 341-347.

26 Le Bars J., Specht U., Bradley J.S., Blackmond D.G. (1999) *Langmuir* **15**, 7621-7625.

27 Rodriguez A., Amiens C., Chaudret B., Casanove M.-J., Lecante P., Bradleu J.S. (1996) *Chem. Mater.* **8**, 1978-1986.

28 Dassenoy F., Philippot K., Ould Ely T., Amiens C., Lecante P., Snoeck E., Mosset A., Casanove M.-J., Chaudret B. (1998) *New J. Chem.* 703-711.

29 De Caro D., Bradley J.S. (1998) *New J. Chem.* 1267-1273.

30 De Caro D., Bradley J.S. (1998) *Langmuir* **14**, 245-247.

31 Lange C., De Caro D., Gamez A., Storck S., Bradley J.S., Maier W.F. (1999) *Langmuir* **15**, 5333-5338.

32 Pan C., Dassenoy F., Casanove M.-J., Philippot K., Amiens C., Lecante P., Mosset A., Chaudret B. (1999) *J. Phys. Chem.* B **103**, 10098-10101.

33 Chan Y.N.C., Craig G.S.W., Schrock R.R., Cohen R.E. (1992) *Chem. Mater.* **4**, 885-894.

34 Arul Dhas N., Cohen H., Gedanken A. (1997) *J. Phys. Chem. B* **101**, 6834-6838.

35 Pery T., Pelzer K., Buntkowsky G., Philippot K., Limbach H.-H., Chaudret B. (2005) *Chem. Phys. Chem.* **6**, 605-607.

36 Pelzer K., Philippot K., Chaudret B. (2003) *Z. Phys. Chem.* **217**, 1539-1547.

37 Pelzer K., Laleu B., Lefebvre F., Philippot K., Chaudret B., Candy J.-P., Basset J.-M. (2004) *Chem. Mater.* **16**, 4937-4941.

38 Ramirez E., Jansat S., Philippot K., Lecante P., Gomez M., Masdeu-Bulto A., Chaudret B. (2004) *J. Organomet. Chem.* **689**, 4601-4610.

39 De Caro D., Ould Ely T., Mari A., Chaudret B., Snoeck E., Respaud M., Broto J.-M., Fert A. (1996) *Chem. Mater.* **8**, 1987-1991.

40 Tran N.T., Powell D.R., Dahl L.F. (2000) *Angew. Chem., Int. Edit.* **39**, 4121-4125.

41 Gomez S., Erades L., Philippot K., Chaudret B., Collière V., Balmes O., Bovin J.-O. (2001) *Chem. Commun.*, 1474-1475.

42 Shah P.S., Husain S., Johnston K.P., Korgel B.A. (2001) *J. Phys. Chem. B* **105**, 9433-9440.

43 Bönnemann H., Braun G.A. (1996) *Angew. Chem. Int. Edit.* **35**, 1992-1995.

44 Gamez A., Kohler J., Bradley J. (1998) *Catal. Lett.* **55**, 73-77.

45 Köhler J.U., Bradley J.S. (1998) *Langmuir* **14**, 2730-2735.

46 Jansat S., Gómez M., Philippot K., Muller G., Guiu E., Claver C., Castillón S., Chaudret B. (2004) *J. Am. Chem. Soc.* **126**, 1592-1593.

47 Son S.U., Jang Y., Yoon K.Y., Kang E., Hyeon T. (2004) *Nanoletters* **4**, 1147-1151.

48 Gomez M., Philippot K., Collière V., Lecante P., Muller G., Chaudret B. (2003) *New J. Chem.* **27**, 114-120.

49 Jansat S., Picurelli D., Pelzer K., Philippot K., Gómez M., Muller G., Lecant P., Chaudret B. (2006) *New J. Chem.* **30**, 115-122.

50 Dupont J., Fonseca G.S., Umpierre A.P., Fichtner P.F.P., Teixera S.R. (2002) *J. Am. Chem. Soc.* **124**, 4228-4229.

51 Fonseca G.S., Umpierre A.P., Fichtner P.F.P., Teixera S.R., Dupont J. (2003) *Chem. Eur. J.* **9**, 3263-3269.

52 Fonseca G.S., Scholten J.D., Dupont J. (2004) *Synlett* **9**, 1525-1528.

53 Scheeren C.W., Machado G., Dupont J., Fichtner P.F.P., Texeira S.R. (2003) *Inorg. Chem.* **42**, 4738-4742.

54 Silveira E.T., Umpierre A.P., Rossi L.M., Machado G., Morais J., Soares G.V., Baumvol I.J.R., Teixeira S.R., Fichtner P.F.P., Dupont J. (2004) *Chem. Eur. J.* **10**, 3734-3740.

55 Cassol C.C., Umpierre A.P., Machado G., Wolke S.I., Dupont J. (2005) *J. Am. Chem. Soc.* **127**, 3298-3299.

56 Vidoni O., Philippot K., Amiens C., Chaudret B., Balmes O., Malm J.-O., Bovin J.-O., Senocq F., Casanove M.-J. (1999) *Angew. Chem. Int. Edit.* **38**, 3736-3738.

57 Pelzer K., Vidoni O., Philippot K., Chaudret B., Collière V. (2003) *Adv. Funct. Mater.* **13**, 118-126.

58 Duan Z., Hampden-Smith M.J. (1992) *Chem. Mater.* **4**, 1146-1148.

59 Osuna J., De Caro D., Amiens C., Chaudret B., Snoeck E., Respaud M., Broto J.-M., Fert A. (1996) *J. Phys. Chem.* **100**, 14571-14574.

60 Dassenoy F., Casanove M.-J., Lecante P., Verelst M., Snoeck E., Mosset A., Ould Ely T., Amiens C., Chaudret B. (2000) *J. Chem. Phys.* **112**, 8137-8145.

61 Billas I.M.L., Châtelain I.M.L., de Heer W.A. (1994) *Science* **265**, 1682-1684.

62 Respaud M., Broto J.-M., Rakoto H., Fert A.R., Thomas L., Barbara B., Verelst M., Snoeck E., Lecante P., Mosset A., Osuna J., Ould Ely T., Amiens C., Chaudret B. (1998) *Phys. Rev. B* **57**, 2925-2935.

63 De Caro D., Bradley J.S. (1997) *Langmuir* **13**, 3067-3069.

64 Ould Ely T., Amiens C., Chaudret B. (1999) *Chem. Mater.* **11**, 526-529.

65 Cordente N., Amiens C., Chaudret B., Respaud M., Senocq F., Casanove M.-J. (2003) *J. Appl. Phys.* **94**, 6358-6365.

66 Ould Ely T., Pan C., Amiens C., Chaudret B., Dassenoy F., Lecante P., Casanove M.-J., Mosset A., Respaud M., Broto J.-M. (2000) *J. Phys. Chem. B* **104**, 695-702.

67 Zitoun D., Amiens C., Chaudret B., Fromen M.-C., Lecante P., Casanove M.-J., Respaud M. (2003) *J. Phys. Chem. B* **107**, 6997-7005.

68 Zitoun D., Respaud M., Fromen M.-C., Lecante P., Casanove M.-J., Amiens C., Chaudret B. (2004) *J. Magn. Magn. Mater.* **272-276**, 1536-1538.

69 Dumestre F., Chaudret B., Amiens C., Fromen M.-C., Casanove M.-J., Renaud P., Zurcher P. (2002) *Angew. Chem. Int. Edit.* **41**, 4286-4289.

70 Dumestre F., Chaudret B., Amiens C., Respaud M., Fejes P., Renaud P., Zurcher P. (2003) *Angew. Chem. Int. Edit.* **42**, 5213-5216.

71 Snoeck E., Dunin-Borkowski R.E., Dumestre F., Renaud P., Amiens C., Chaudret B., Zurcher P. (2003) *Appl. Phys. Lett.* **82**, 88-90.

72 Dumestre F., Chaudret B., Amiens C., Renaud P., Fejes P. (2004) *Science* **303**, 821-823.

73 Cordente N., Respaud M., Senocq F., Casanove M.-J., Amiens C., Chaudret B. (2001) *Nano Lett.* **1**, 565-568.

74 Dumestre F., Martinez S., Zitoun D., Fromen M.-C., Casanove M.-J., Lecante P., Respaud M., Serres A., Benfield R., Amiens C., Chaudret C. (2004) *Faraday Discuss.* **125**, 265-278.

75 Desvaux C., Amiens C., Fejes P., Renaud P., Respaud M., Lecante P., Snoeck E., Chaudret B. (2005) *Nature Mat.*, 1-4.

76 De Caro D., Agelou V., Duteil A., Chaudret B., Mazel R., Roucau C., Bradley J.S. (1995) *New J. Chem.* **19**, 1265-1274.

77 De Caro D., Wally H., Amiens C., Chaudret B. (1994) *J. Chem. Soc. Chem. Commun.* 1891-1892.

78 Hambrock J., Becker R., Birkner A., Weiss J., Fischer R.A. (2002) *Chem. Commun.*, 68-69.

79 Rataboul F., Nayral C., Casanove M.-J., Maisonnat A., Chaudret B. (2002) *J. Organomet. Chem.* **643-644**, 307-312.

80 Hambrock J., Schröter M.K., Birkner A., Wöll C., Fischer R.A. (2003) *Chem. Mater.* **15**, 4217-4222.

81 Soulantica K., Maisonnat A., Fromen M.-C., Casanove M.-J., Lecante P., Chaudret P. (2001) *Angew. Chem. Int. Edit.* **40**, 448-451.

82 Soulantica K., Maisonnat A., Senocq F., Fromen M.-C., Casanove M.-J., Chaudret P. (2001) *Angew. Chem. Int. Edit.* **40**, 2983-2986.

83 Soulantica K., Erades L., Sauvan M., Senocq F., Maisonnat A., Chaudret B. (2003) *Adv. Funct. Mater.* **13**, 553-557.

84 Soulantica K., Maisonnat A., Fromen M.-C., Casanove M.-J., Chaudret B. (2003) *Angew. Chem. Int. Edit.* **42**, 1945-1949.

85 Nayral C., Viala E., Fau P., Senocq F., Jumas J.-C., Maisonnat A., Chaudret B. (2000) *Chem. Eur. J.* **6**, 4082-4090.

86 Fau P., Sauvan M., Trautweiler S., Nayral C., Erades L., Maisonnat A., Chaudret B. (2001) *Sensor. Actuat. B - Chem.* **78**, 83-88.

87 Schneider J.J., Czap N., Hagen J., Ensling J., Gütlich P., Reinoehl U., Bertagnolli H., Luis F., de Jongh L.J., Wark M., Grubert G., Hornyak G.L., Zanoni R. (2000) *Chem. Eur. J.* **6**, 4305-4321.

88 Tang J., Redl F., Zhu Y., Siegrist T., Brus L.E., Steigerwald M.L. (2005) *Nanoletter* **5**, 543-548.

89 Shim M., Guyot-Sionnest P. (2001) *J. Am. Chem. Soc.* **123**, 11651-11654.

90 Monge M., Kahn M.L., Maisonnat A., Chaudret B. (2003) *Angew. Chem. Int. Edit.* **42**, 5321-5324.

91 Kahn M.L., Monge M., Collière V., Senocq F., Maisonnat A., Chaudret B. (2005) *Adv. Funct. Mater.* **15**, 458-468.

92 Kahn M.L., Monge M., Snoeck E., Maisonnat A., Chaudret B. (2005) *Small* **1**, 221-224.

93 Kim C.G., Sung K., Chung T.M., Jung D.Y., Kim Y. (2003) *Chem. Commun.*, 2068-2069.

94 Pelzer K., Philippot K., Chaudret B., Meyer-Zaika W., Schmid G. (2003) *Z. Anorg. Allg. Chem.* **629**, 1217-1222.

95 Kormann H.-P., Schmid G., Pelzer K., Philippot K., Chaudret B. (2004) *Z. Anorg. Allg. Chem.* **630**, 1913-1918.

96 Hulea V., Brunel D., Galarneau A., Philippot K., Chaudret B., Kooyman P.J., Fajula F. (2005) *Micropor. Mesopor. Mat.* **79**, 185-194.

97 Guari Y., Thieuleux C., Mehdi A., Reyé C., Corriu R.J.P., Gomez-Gallardo S., Philippot K., Chaudret B., Dutartre R. (2001) *Chem. Commun.,* 1374-1375.

98 Guari Y., Thieuleux C., Mehdi A., Reyé C., Corriu R.J.P., Gomez-Gallardo S., Philippot K., Chaudret B. (2003) *Chem. Mater.,* 2017-2024.

99 Guari Y., Soulantica K., Philippot K., Thieuleux C., Mehdi A., Reyé C., Chaudret B., Corriu R.J.P. (2003) *New J. Chem.,* 1029-1031.

100 Jansat S., Pelzer K., García-Antoń J., Raucoules R., Philippot K., Maisonnat A., Chaudret B., Guari Y., Medhi A., Reyé C., Corriu R.J.P. (2007) Adv. Funct. Mater., **17**, 3339-3347.

101 Desportes S., Steinmetz D., Hémati M., Philippot K., Chaudret B. (2005) *Powder Technol.* **15**, 12-19.

Final manuscript received in July 2007